



# CHORUS

This is the accepted manuscript made available via CHORUS. The article has been published as:

## Angular momentum distribution in Rydberg states excited by a strong laser pulse

J. Venzke, R. Reiff, Z. Xue, A. Jaroń-Becker, and A. Becker

Phys. Rev. A **98**, 043434 — Published 30 October 2018

DOI: [10.1103/PhysRevA.98.043434](https://doi.org/10.1103/PhysRevA.98.043434)

# Angular momentum distribution in Rydberg states excited by a strong laser pulse

J. Venzke,<sup>1</sup> R. Reiff,<sup>1</sup> Z. Xue,<sup>1</sup> A. Jaroń-Becker,<sup>1</sup> and A. Becker<sup>1</sup>

<sup>1</sup>*JILA and Department of Physics, University of Colorado, Boulder, Colorado 80309-0440, USA*

We study the excitation to Rydberg states in the interaction of the hydrogen atom with a short strong laser pulse. Utilizing solutions of the time-dependent Schrödinger equation we find that the parity of the populated angular momentum states agrees with the selection rules for multiphoton resonant absorption at low intensities, if the pulse length is not too short. In contrast, the parity effect cannot be observed for ultrashort pulses as well as for long pulses at high intensities. We further identify signatures of the population in the excited states via the line emissions from the populated  $np$  states after the end of the pulse exhibiting the parity effect.

PACS numbers: 32.80.Fb, 32.80.Rm

## I. INTRODUCTION

Fundamental processes in strong-field atomic physics are above-threshold ionization (ATI), high harmonic generation (HHG) and non-sequential double ionization. These highly nonlinear processes are induced by the absorption of multiple photons from the laser field, which in the limit of a large photon number can also be described as a tunneling process. Excitation of the atom is known to play an important role in each of the processes. It has been initially observed via resonant enhancement in the population of excited states [1, 2] and structures in the energy spectrum [3–5] and in energy-resolved angular distributions [6] of photoelectrons. These resonance effects have been explained by multiphoton absorption through Rydberg states, which are AC-Stark shifted in the presence of a laser field. More recently, significant excitation of atoms has also been observed in the tunneling regime and described by the frustrated tunneling ionization model [7].

The latter observation has renewed the general interest in the mechanisms leading to the population of excited (Rydberg) states during the interaction of an atom with an intense laser pulse (most recently, e.g., in Refs. [8–32]). The important role of Rydberg states in various strong-field ionization processes and harmonic generation has been discussed. For example, resonant enhancement of below-threshold harmonics [8, 12, 33], emission from excited states via free induction decay [12, 23], high harmonic emission through ionization from excited states and recombination to the ground state [23, 34] have been predicted and observed.

Recent theoretical studies of the excitation mechanism in strong fields mainly consider the distribution of the population as a function of the principal quantum number of the excited states [9, 10, 25, 31, 32]. It was shown that the modulation of the excitation probability is related to the channel closing effect [9, 10, 32, 35]. The latter phenomenon occurs at threshold intensities at which the absorption of one more photon is needed to ionize the atom due to the shift of the ionization threshold by the ponderomotive energy. The interpretation that an increase in excitation can be understood as result of the

shift of the first ATI peak below the ionization threshold [9, 10] is in agreement with the explanation of earlier experimental results (e.g., [2, 3, 6]) via the resonance-enhanced population of AC-Stark shifted excited states.

Theoretical analysis of the angular momentum distribution in the populated Rydberg states is less advanced. Predictions of Floquet theory for a monochromatic laser field [35] and results of numerical calculations for laser pulses with a trapezoidal envelope [32] yield that the angular momentum of the excited Rydberg states has the same parity as  $N_p - 1$ , where  $N_p$  is the minimum number of photons needed to ionize the atom. Furthermore, the angular quantum number of the states with the largest population in numerical calculations [9, 10, 32] agrees well with semiclassical estimations [36], initially performed for low-energy angular resolved photoelectron distributions.

In this work we extend the previous analysis by considering excitation in laser pulses with sine squared and Gaussian envelopes. This gives us the opportunity to study if the parity of the populated angular momentum states in such pulses agrees with the selection rules obtained for monochromatic fields and how the results depend on the pulse length at low and high intensities. In the second part we investigate how the population of angular momentum states leaves its footprints in the radiation generated via transitions from the excited states to the ground state. For our studies we make use of results of numerical solutions of the time-dependent Schrödinger equation (TDSE) for the interaction of the hydrogen atom with an intense linearly polarized laser pulse.

The paper is organized as follows: In Sec. II we briefly discuss theoretical aspects of the excitation process in strong fields as well as the numerical methods used for the solutions of the time-dependent Schrödinger equation. In Sec. III we present numerical results for angular momentum distributions in resonantly excited states. In particular, we focus on the effects of intensity and pulse length on the distribution. Finally, in Sec. IV, numerical results for the high harmonic generation spectra are presented and analyzed in view of signatures of the population in the excited states. We summarize our results in Sec. V. We use Hartree atomic units,  $e = m = \hbar = 1$ ,

throughout the article unless stated otherwise.

## II. THEORETICAL CONSIDERATIONS AND NUMERICAL METHODS

We are solving the time-dependent Schrödinger equation (TDSE) for the interaction of an atom with a linearly polarized intense laser pulse in the velocity gauge:

$$i\frac{\partial}{\partial t}\psi(\mathbf{r}, t) = \left[ \frac{\mathbf{p}^2}{2} - \frac{\mathbf{A}(t) \cdot \mathbf{p}}{c} + V(\mathbf{r}) \right] \psi(\mathbf{r}, t) \quad (1)$$

where  $\mathbf{p}$  is the momentum operator and  $V$  is the single-active-electron atomic potential; here we have chosen atomic hydrogen ( $V(r) = -1/r$ ). In this work we set the vector potential of the laser field as:

$$A(t) = A_0 f(t) \sin(\omega_A(t - \tau/2) + \phi_A) \quad (2)$$

where  $A_0 = \frac{c\sqrt{I}}{\omega_A}$ , and  $\tau = \frac{2\pi N}{\omega_A}$  and  $c$  is the speed of light,  $I$  is the peak intensity,  $N$  is the number of cycles in the pulse, and  $\phi_A$  is the carrier-to-envelope phase, which is set to  $\phi_A = 0$  if not mentioned otherwise.  $\omega_A$  is the central frequency, which is chosen such that the spectral distribution of the  $E$ -field peaks at the frequency  $\omega_E$  corresponding to a wavelength of 800 nm. The results of this paper are obtained utilizing sine squared:

$$f(t) = \sin^2\left(\frac{\pi t}{\tau}\right) \quad (3)$$

and Gaussian:

$$f(t) = \exp\left(-\ln(2)\left(\frac{2(t - \tau/2)}{\tau}\right)^2\right) \quad (4)$$

envelope functions.

We utilize a second order finite difference method in cylindrical coordinates for the spatial derivatives. Time propagation is often performed using the split-operator method where the Hamiltonian ( $\hat{H}$ ) split into its spatial dimensions, e.g. along ( $z$ ) and perpendicular ( $\rho$ ) to the laser polarization direction. The resulting propagation scheme is

$$\psi(\mathbf{r}, t + \Delta t) \approx e^{-i\hat{H}_\rho \frac{\Delta t}{2}} e^{-i\hat{H}_z(t)\Delta t} e^{-i\hat{H}_\rho \frac{\Delta t}{2}} \psi(\mathbf{r}, t). \quad (5)$$

where

$$e^{-i\hat{H}\Delta t} \approx \frac{1 - i\frac{\Delta t}{2}\hat{H}}{1 + i\frac{\Delta t}{2}\hat{H}} \quad (6)$$

produces a set of tridiagonal matrices which can be solved with  $\mathcal{O}(\mathcal{N})$  operations and  $\mathcal{O}(\mathcal{N})$  memory. However, parallelization of such a method on a modern supercomputer with distributed memory can be cumbersome, requiring multiple all-to-all Message Passing Interface (MPI) messages during each time step.

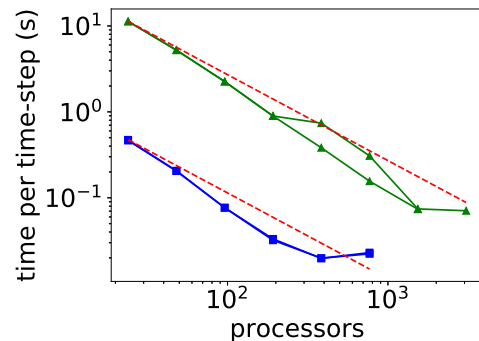


FIG. 1: (Color online) Scaling results for present Crank-Nicolson method. Two runs each for calculations with 1 million (blue with squares) and 15 million grid points (green with triangles) have been performed. Note that the scaling improves with increasing number of grid points. The actual calculations in the present paper involved grids with over 112 million grid points.

Instead, we avoid splitting the Hamiltonian and propagate the total Hamiltonian in time using a second order Crank-Nicolson scheme where

$$\psi(\mathbf{r}, t + \Delta t) \approx e^{-i\hat{H}\Delta t}\psi(\mathbf{r}, t). \quad (7)$$

We note that the Crank-Nicolson method is not tridiagonal and a direct solution would require  $\mathcal{O}(\mathcal{N}^3)$  operations and  $\mathcal{O}(\mathcal{N}^2)$  memory which is significantly more than in the split operator method. However, the system of equations in the full Crank-Nicolson method is sparse and iterative methods can be used to vastly accelerate the time propagation. We utilize the Generalized Minimal Residual Method (GMRES), implemented in PETSc [37, 38], which solves the sparse system of linear equations in  $\mathcal{O}(\mathcal{N} \log(\mathcal{N}))$  operations and  $\mathcal{O}(\mathcal{N})$  memory. The PETSc library makes it straightforward to parallelize the Crank-Nicolson method on modern supercomputers with distributed memory. On a local supercomputer (Summit, CU Boulder), we achieved super-linear scaling up to 3,000+ cores (Fig. 1) allowing us to complete simulations in a matter of hours that would take weeks running on a high-end workstation. We tested the convergence of the present computation scheme with respect to time and spatial steps. As an example, we present in Fig. 2 a comparison of results for the high harmonic spectrum generated from a hydrogen atom interacting with an eight-cycle linearly polarized laser pulse at 800 nm and a peak intensity of  $10^{14}$  W/cm<sup>2</sup>, obtained using (a) two different spatial steps, (b) two different temporal steps and (c) using the present Crank-Nicolson scheme and using the split-operator method.

Real space methods do not provide direct access to the populations of excited states. In order to extract the populations in the Rydberg states, we project the final wavefunction on a large number of bound states calculated on the grid. We use the Krylov-Schur method

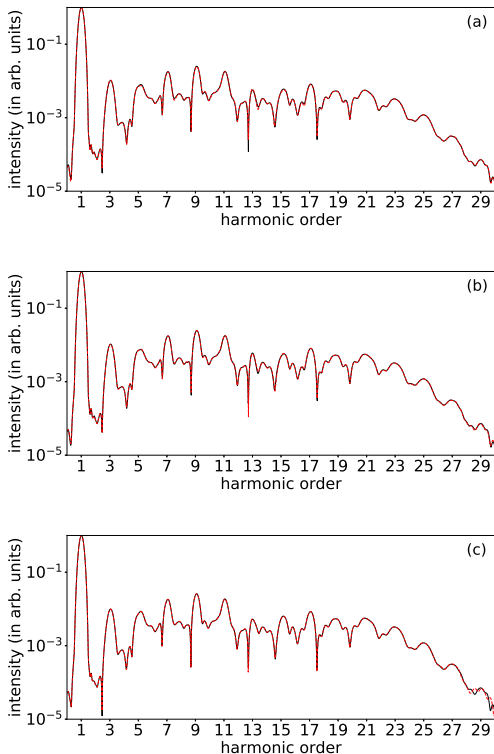


FIG. 2: (Color online) Comparison of high harmonic spectra: (a) obtained using a spatial step of  $\Delta \equiv \Delta z = \Delta \rho = 0.1$  (red dashed-line) and  $\Delta = 0.08$  (black line) with a temporal steps  $\Delta t = \frac{\Delta^2}{2}$ , (b) obtained using a temporal step of  $\Delta t = 0.15$  (red dashed-line) and  $\Delta t = \frac{\Delta^2}{2} = 0.005$  (black line) and spatial steps  $\Delta = 0.1$ , and (c) obtained using the present full Crank-Nicolson scheme (black line) and an independently developed split-operator method (red dashed-line) with  $\Delta t = 0.00125$  and  $\Delta = 0.05$  for both simulations.

provided in the SLEPc library [39, 40] to calculate bound states (up to  $n = 14$  in the present set of calculations) on the spatial grid. We have ensured that the bound states studied in this work fit inside the real space portion of our grid. Thus, the populations are not artificially changed by the boundary conditions that require the wavefunction to go to zero at the edge of the grid. We utilize an exterior complex scaling (ECS) potential to absorb outgoing wave packets.

In all calculations presented below we used a grid ranging up to  $\rho = 750$  a.u. and  $z = \pm 750$  a.u. with a grid spacing of  $\Delta = 0.1$  a.u. in both directions and a time step of  $\Delta t = 0.15$  a.u. We use the outer 37.5 a.u. of the grid in both directions for the ECS potential. This grid can easily fit bound states up to  $n = 14$  within the real portion of the grid. In Fig. 3 we show examples of excited states with the largest principal quantum number analyzed in the present work.

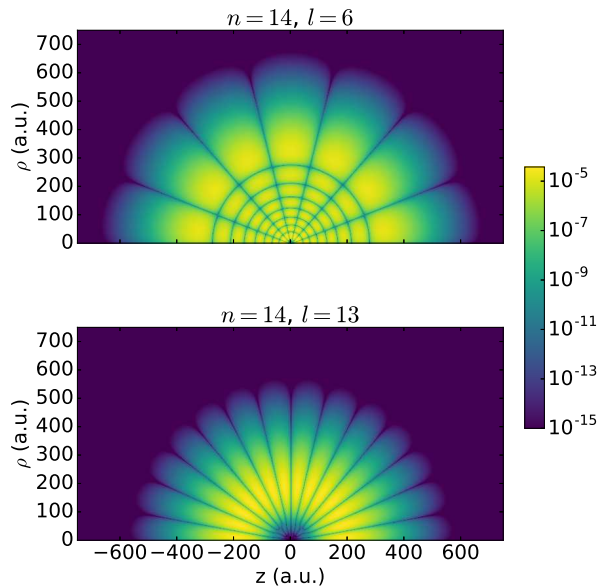


FIG. 3: (Color online) Representation of excited states on the grid in cylindrical coordinates:  $n = 14$ ,  $l = 6$  (upper panel) and  $n = 14$ ,  $l = 13$  (lower panel).

### III. ANGULAR MOMENTUM DISTRIBUTIONS

#### A. Parity effect in pulses

We study the angular momentum distribution in Rydberg states of the hydrogen atom. To this end, we consider processes during which these states are shifted into resonance with multiphoton absorption from the initial ground state of the atom (with energy  $E_i$ ). Assuming that the energy shift of high lying excited states under the influence of an intense laser field is approximately equal to the ponderomotive shift [5] and the shift occurs instantaneously during the pulse [41], the intensity for a  $N_p$  photon process to resonantly excite approximately with an excited state with energy  $E_n$  is given by:

$$I = 4\omega_E^2(N_p\omega_E + E_i - E_n). \quad (8)$$

In our calculations we have considered peak intensities such that the  $n = 8$  states are in resonance at central frequency  $\omega_E$ , corresponding to a wavelength of 800 nm, with  $N_p = 10, 11, \dots, 15$  photon processes. Since we study the interaction with laser pulses, instead of monochromatic fields, more than one manifold of states can be resonantly excited. For example, the bandwidth of a 20 cycle sine squared pulse at 800 nm covers all excited states  $n \gtrsim 6$  within the same  $N_p$  photon process. We further note that in the present cases, the  $n = 3$  and  $n = 2$  states are approximately resonant via  $N_p - 1$  and  $N_p - 2$  photon processes, respectively, assuming that the energy shift of these states equals the ponderomotive energy as well.

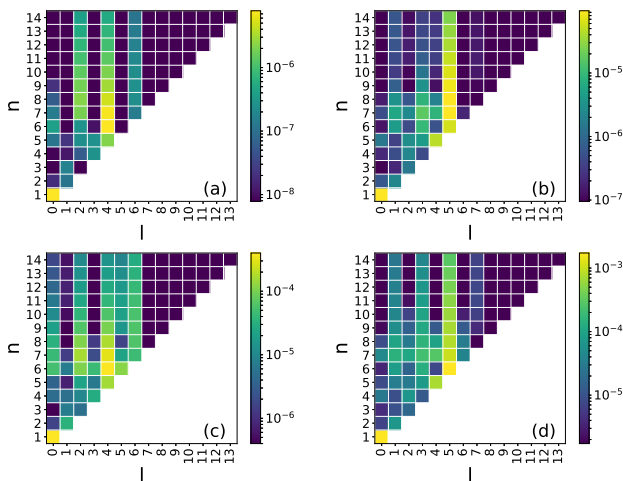


FIG. 4: (Color online) Excited state distribution as function of  $n$  (vertical axis) and  $l$  (horizontal axis) at the end of 20 cycle pulses with sin squared envelope and peak intensities: (a)  $I_0 = 3.4 \times 10^{13}$  W/cm<sup>2</sup>, (b)  $I_0 = 6.0 \times 10^{13}$  W/cm<sup>2</sup>, (c)  $I_0 = 8.6 \times 10^{13}$  W/cm<sup>2</sup>, and (d)  $I_0 = 1.12 \times 10^{14}$  W/cm<sup>2</sup>. Left (right) column corresponds to cases in which the Rydberg states are resonant with an even (odd) number of photons.

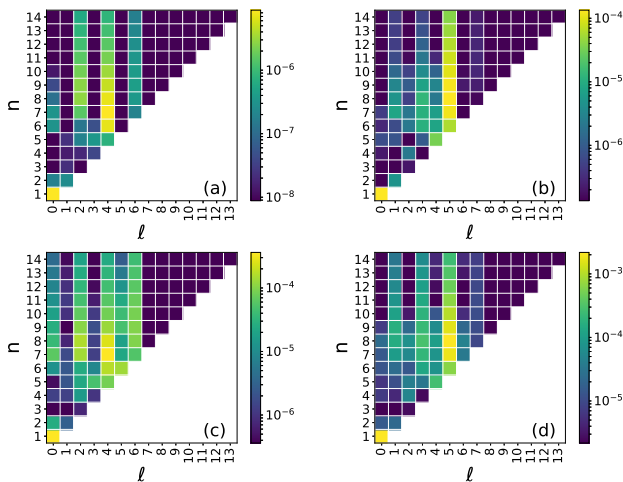


FIG. 5: (Color online) Same as Fig. 4 but for pulses with Gaussian envelope and 14 cycles FWHM. The pulse duration approximately matches that for the sine-squared pulses in Fig. 4 at FWHM.

The population in each quantum state ( $n, l$ ) at the end of the pulse is shown in Fig. 4 (20 cycle pulses with sine-squared envelope) and Fig. 5 (14 FWHM cycle pulses with Gaussian envelope) for intensities between  $10^{13}$  and  $10^{14}$  W/cm<sup>2</sup>. The results shown in the left (right) column correspond to cases in which the Rydberg states are resonant with an even (odd) number of photons. In all cases we see that the highest angular momentum states ( $l > 7$ ) are not much populated, in agreement with previous studies [32] and semiclassical estimates [36]. In the results we indeed observe signatures of the selection

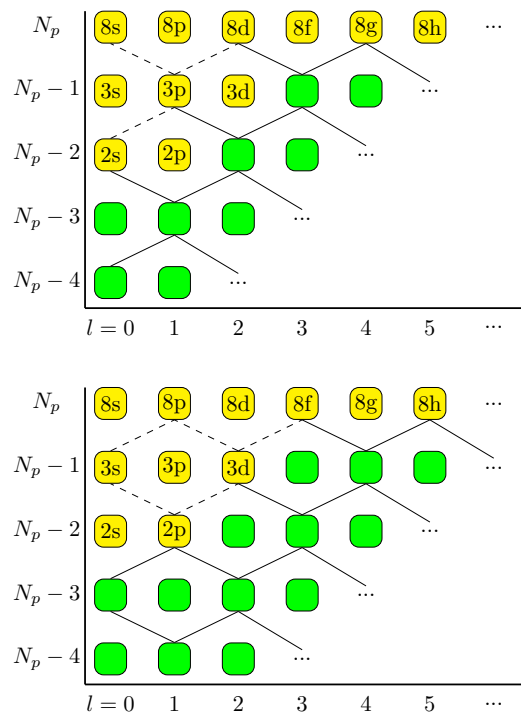


FIG. 6: (Color online) The absorption pathways in an even (odd) photon process in the top (bottom) panel. Green squares represent virtual states with energy  $N\omega$  above the ground state and angular momentum  $l$ . The yellow squares represent real states labeled by the quantum numbers. Solid lines refer to open pathways while dashed lines represent pathways which are suppressed due to population trapping in a lower excited state.

rules resulting in dominant population of states with an even (odd) angular momentum quantum number for the absorption of even (odd) photons in the plots on the left (right). This shows that in the intensity regime of  $10^{13}$  to  $10^{14}$  W/cm<sup>2</sup> the parity selection rules, previously studied for monochromatic fields and flat-top pulses, are effective for long pulses of about 20 cycles. Since the parity effect is found to occur independent of the form of the envelope we restrict ourselves below to pulses with sine-squared envelope. However, we observe that the contrast between the population in even and odd states is stronger at lower intensities. We will further discuss this aspect in subsection III B.

The results also show that for an odd parity process (right column) predominantly one angular momentum state ( $l = 5$ ) is populated. This is in agreement with the results presented by Li et al. [10], who conjectured that electrons in the low angular momentum states more easily absorb additional photons resulting in suppression of population in these states due to ionization. However, our results for even parity processes exhibit a pattern, alternating in  $l$ , showing that both low and high angular momentum states, except for the  $s$ -states, remain populated at the end of the pulse.

We therefore put forward an alternative explanation.

To this end, in Fig. 6 we show the various pathways leading to a resonant population in the  $n = 8$  (and the other Rydberg) states for absorption of an even (top panel) or an odd (bottom panel) number of photons, termed by  $N_p$ . Starting from the  $1s$  ground state, the absorption of successive photons proceeds through virtual states (depicted via empty green squares in Fig. 6), following the selection rule  $\Delta l = \pm 1$ . As mentioned above, for the hydrogen atom and a pulse at a central wavelength of 800 nm the (shifted)  $n = 3$  and  $n = 2$  states are approximately resonant via  $N_p - 1$  and  $N_p - 2$  photon processes, as shown in Fig. 6 (real states are depicted by yellow squares labeled with quantum number  $nl$ ). Assuming that the resonant transitions to lower lying energy levels cause a trapping of population in these states, further absorption from these states will be suppressed. Such suppressed pathways are denoted by dashed lines in Fig. 6, while other (open) pathways are represented by solid lines. Following the pathways, we see that in the manifold of the Rydberg levels for an even number photon process (top panel) the  $l = 2$  state is partially and the  $l = 4, 6, \dots$  states are fully accessible, while the  $l = 0$  ( $s$ -state) should be suppressed, which is in agreement with the pattern, alternating in  $l$ , that we observe in Figs. 4 and 5 (left columns). In contrast, for an odd number photon process (bottom panel) the pathways to the  $l = 1$  states are strongly and those to the  $l = 3$  states are partially suppressed, making the states with  $l = 5$  state the first fully accessible states among the Rydberg levels, in agreement with the results presented in Figs. 4 & 5 (right columns).

### B. Short vs. long pulses and CEP effects

The time-frequency uncertainty relation yields that a pulse spectrum broadens as the number of optical cycles decreases. Consequently, in an ultrashort pulse an excited state can be reached via absorption of different number of photons. Due to this mix of even and odd number of photon processes one may expect that in such pulses a separation in population of odd vs. even angular momentum quantum states cannot be achieved. This is confirmed by the results of our numerical calculations at low and high intensities, shown in Fig. 7(a) and (d). For a 2 cycle pulse there is a smooth distribution over the lower angular momentum states for each principal quantum number at low ( $3.4 \times 10^{13}$  W/cm<sup>2</sup>, panel (a)) and high ( $1.64 \times 10^{14}$  W/cm<sup>2</sup>, panel (d)) peak intensity.

In contrast, the narrowing of the energy spectrum as pulse duration increases does not necessarily lead to an increase of the population in the angular momentum states of one parity over the other. For the low intensity 10-photon resonant process ( $3.4 \times 10^{13}$  W/cm<sup>2</sup>, Fig. 7, upper row) we observe in the numerical results that Rydberg states with a well defined angular momentum parity are predominantly populated when the pulse duration is increased to 10 and 20 cycles. On the other hand,

at the higher intensity ( $1.64 \times 10^{14}$  W/cm<sup>2</sup>, Fig. 7, lower row) we observe some contrast between the population in the angular momentum states of different parity for the 10 cycle pulse (panel (e)), while the differences in the population of the different channels further blurs when the duration is increased to 20 cycles (panel (f)).

Within the interpretation of resonant excitation the loss of the parity effect for long pulses with high peak intensities can be understood as follows. At the higher peak intensity, the highly excited states are shifted into resonance for 10-14 photon processes over the rising and trailing parts of the pulse, before they are resonantly excited with a 15 photon process at the peak intensity. Although the excitation probability raises with an increase of the intensity during the pulse, the time intervals over which the states are in resonance with a certain photon-order process increase with the pulse length. Thus, there is a significant excitation of the Rydberg states due to the absorption of odd as well as even numbers of photons in a pulse at high peak intensity and long duration.

Furthermore, excitation channels driven by absorption of different numbers of photons with the same parity may interfere, leading to the enhancement or suppression of population in certain angular momentum states and the loss of the parity effect. Interference effects in excitation have been studied extensively in the few-photon regime. Among others, it has been shown that the excitation probabilities can be controlled via the carrier envelope phase (CEP) of the pulse, even in the long pulse limit (e.g., [42, 43]). We observe in the results presented in Fig. 8 that the population distribution in the angular momentum states driven by the present more complex multiphoton processes indeed changes significantly with variation of the CEP at high intensities, indicative of potential interference effects.

However, we note that there may exist alternative explanations for the loss of the parity effect in the distribution at long pulses with high peak intensity. For example, in the tunneling regime the mechanism of frustrated ionization has been explored [7]. According to that mechanism highly excited states are populated during the trailing edge of the pulse by deceleration of the electron over many laser cycles and electron recapturing once the laser pulse ceases. Since excited states of any angular momentum can be populated during the recapturing, the loss of the parity effect for long pulses at intensities in the tunneling regime is consistent with the frustrated ionization mechanism as well.

## IV. RADIATION SPECTRA

It has recently been discussed [8, 12, 23] that the population of excited Rydberg states leads to the emission of radiation due to the transition from the excited states into the ground state, which can be observed in the below-threshold part of high harmonic spectra. In the case of atomic hydrogen such emission is associated with

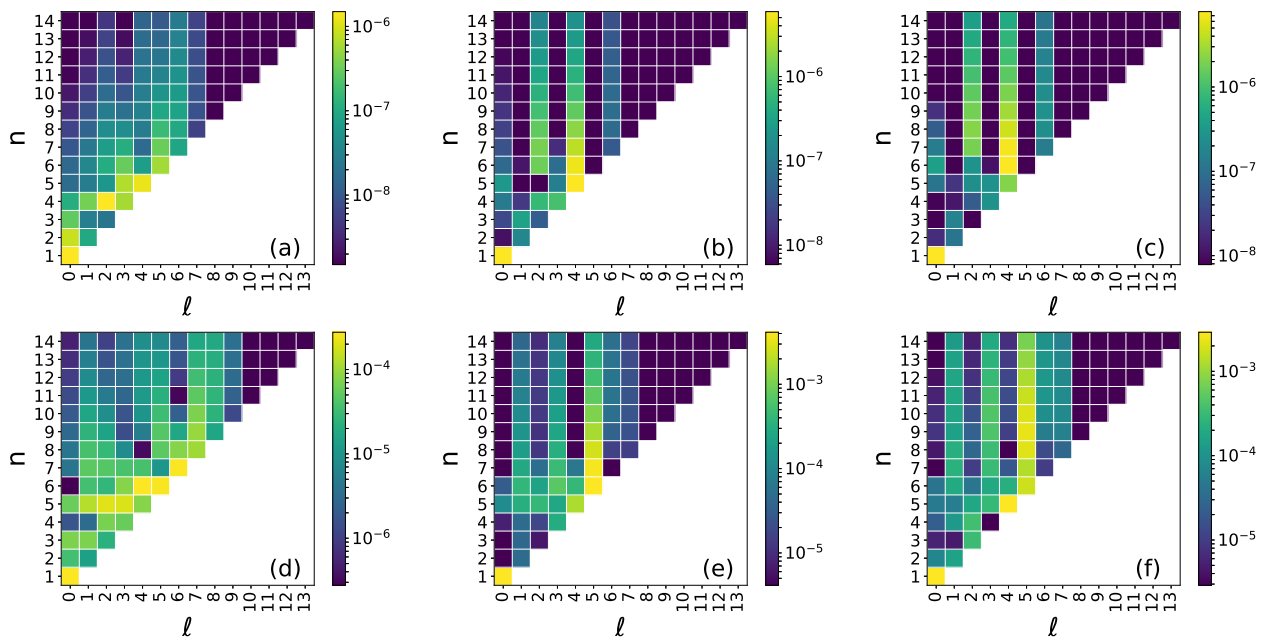


FIG. 7: (Color online) Excited state distribution as function of  $l$  (horizontal axis) and  $n$  (vertical axis) at the end of 2 cycle (panels on left), 10 cycle (panels in middle), and 20 cycle (panels on right) pulses, at low peak intensity  $I_0 = 3.4 \times 10^{13}$  W/cm<sup>2</sup> (top row), and high peak intensity  $I_0 = 1.64 \times 10^{14}$  W/cm<sup>2</sup> (bottom row).

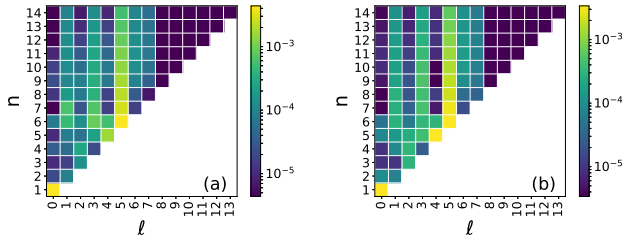


FIG. 8: (Color online) Population of excited states from a 20 cycle pulse with peak intensity of  $I_0 = 1.64 \times 10^{14}$  W/cm<sup>2</sup> and CEP of  $\phi_A = 0.204\pi$  (a) and  $\phi_A = 0.882\pi$  (b)

an excitation of the  $np$  states. In view of the parity effect in the excitation of the Rydberg states according to the absorption of an even or odd number of photons, we expect that the emission may be enhanced or suppressed in certain intensity regimes.

To allow for the separation between the field induced and field free radiation we have calculated the high harmonic spectrum from the dipole acceleration  $a(t)$  such that

$$f_{HHG}(\omega; t_f) \propto \int_{-\infty}^{t_f} a(t') e^{-i\omega t'} dt'. \quad (9)$$

In Fig. 9 we present the radiation spectrum in the region of the 7th and 9th harmonics produced by a 20 cycle, sin squared, 800 nm pulse at intensities (a)  $I_0 = 3.4 \times 10^{13}$  W/cm<sup>2</sup>, (b)  $I_0 = 6.0 \times 10^{13}$  W/cm<sup>2</sup>,

and (c)  $I_0 = 1.64 \times 10^{14}$  W/cm<sup>2</sup>. In each panel the red dashed line shows the spectrum generated during the pulse ( $t_f = \tau$ ) while the black solid line includes free propagation after the pulse has ended ( $t_f = 2\tau$ ). The difference between the two spectra exhibits the radiation related to the transitions from the populated excited  $np$  states at the end of the pulse to the ground state, which has previously been identified in both experiment [8] and macroscopic simulations [12, 23].

Comparison of the spectra obtained at the two intensities clearly exhibits the expected difference in the features related to the parity effect in the population of the Rydberg states. At an intensity of  $3.4 \times 10^{13}$  W/cm<sup>2</sup> (Fig. 9a), the (shifted) Rydberg energy levels are resonantly excited with a 10 photon process leading to population of the even angular momentum states (c.f., Fig. 3(a)). Consequently, the spectrum is free of line emission from the almost unpopulated Rydberg  $p$ -states while we find a strong line corresponding to the strongly populated  $3p$  state, which is near resonant with a 9 photon process. In contrast, by shifting the states by the energy of an additional photon, at an intensity of  $6.0 \times 10^{13}$  W/cm<sup>2</sup> (Fig. 9(b)) we observe a rich line emission spectrum just below the 9th harmonic line emissions from the  $np$ -states, that are resonantly populated by a 11 photon process (Fig. 3(b)). We note that the  $6p$  and  $7p$  states are the most populated  $np$  states and as a result have the strongest emission lines. On the other hand the line corresponding to the  $3p$  state, which cannot be populated by absorption of 10 photons, is strongly suppressed.

As discussed in section III B, at the highest intensity

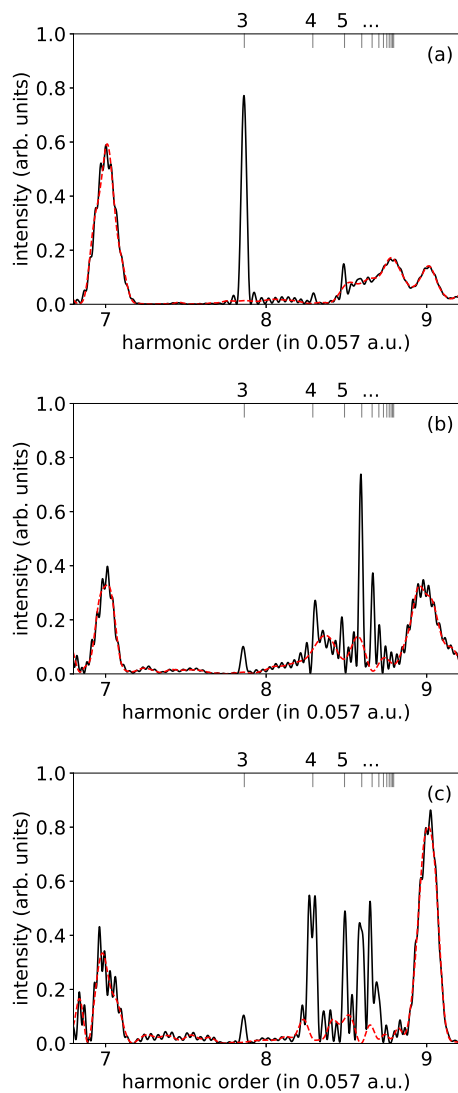


FIG. 9: (Color online) Radiation spectra generated during the pulse (red dashed lines) and those including line emissions after the pulse (black solid lines) are shown for peak intensities: (a)  $I_0 = 3.4 \times 10^{13} \text{ W/cm}^2$ , (b)  $I_0 = 6.0 \times 10^{13} \text{ W/cm}^2$ , and (c)  $I_0 = 1.64 \times 10^{14} \text{ W/cm}^2$ . The vertical gray lines show the field free energy differences between the  $np$  energy levels (up to  $14p$ ) and the  $1s$  ground state.

$I_0 = 1.64 \times 10^{14} \text{ W/cm}^2$ , the population distribution in the angular momentum well defined parity begins to blur. This leads to a relatively even population in states with principle quantum number 4 to 14 seen in (Fig. 7(f)). As a result, we see in Fig. 9(c) line emission from all populated  $np$  states with similar strengths for the states resolved in our spectrum.

## V. SUMMARY

We have analyzed the angular momentum distribution in the Rydberg states of a hydrogen atom excited by a short strong laser pulse, based on numerical results of the time dependent Schrödinger equation, which we solved using a second order Crank-Nicolson scheme. At low intensities the pattern in the population across the angular momentum states can be explained via a parity effect due to the selection rules in multiphoton absorption along with the suppression of pathways due to population trapping in low excited states, if the applied laser pulse is not too short. At high intensities the parity effect gets lost even for long pulses, potentially since the Rydberg states are in resonance with photon processes of different orders for a significant time during the rising and trailing parts of the pulse. The parity effect can be observed in the strengths of the line emissions from the  $np$  states emitted after the end of the pulse.

## Acknowledgments

This work was primarily supported (J.V., R.R., A.B) by a grant from the U.S. Department of Energy, Division of Chemical Sciences, Atomic, Molecular and Optical Sciences Program (Award No. DE-SC0001771). Z.X. was supported by a grant from the U.S. National Science Foundation (Grant No. PHY-1734006). A.J.-B. acknowledges support by AFOSR MURI (Grant No. FA9550-16-1-0121). This work utilized the RMACC Summit supercomputer, which is supported by the National Science Foundation (awards ACI-1532235 and ACI-1532236), the University of Colorado Boulder, and Colorado State University. The Summit supercomputer is a joint effort of the University of Colorado Boulder and Colorado State University.

[1] M.P. de Boer and H.G. Muller, Phys. Rev. Lett. **68**, 2747 (1992).  
 [2] R.R. Jones, D.W. Schumacher, and P.H. Bucksbaum, Phys. Rev. A **47**, R49 (1992).  
 [3] R.R. Freeman, P.H. Bucksbaum, H. Milchberg, S. Darack, D. Schumacher, and M.E. Geusic, Phys. Rev. Lett. **59**, 1092 (1987).  
 [4] M.D. Perry, A. Szoke, and K.C. Kulander, Phys. Rev. Lett. **63**, 1058.

[5] P. Agostini, P. Breger, A. L’Huillier, H.G. Muller, G. Petite, A. Antonetti, and A. Migus, Phys. Rev. Lett. **63**, 2208 (1989).  
 [6] H. Rottke, B. Wolff-Rottke, D. Feldmann, K.H. Welge, M. Dörr, R.M. Potvliege, and R. Shakeshaft, Phys. Rev. A **49**, 4837 (1994).  
 [7] T. Nubbemeyer, K. Gorling, A. Saenz, U. Eichmann, and W. Sandner, Phys. Rev. Lett. **101**, 233001 (2008).  
 [8] M. Chini, X. Wang, Y. Cheng, H. Wang, Y. Wu, E. Cun-

- ningham, P.-C. Li, J. Heslar, D.A. Telnow, S.-I Chu, and Z. Chang, *Nat. Photon.* **8**, 437 (2014).
- [9] Q. Li, X.-M. Tong, T. Morishita, H. Wei, and C.D. Lin, *Phys. Rev. A* **89**, 023421 (2014).
- [10] Q. Li, X.-M. Tong, T. Morishita, C. Jin, H. Wei, and C.D. Lin, *J. Phys. B: At. Mol. Opt. Phys.* **47**, 204019 (2014).
- [11] H. Zimmermann, J. Buller, S. Eilzer, and U. Eichmann, *Phys. Rev. Lett.* **114**, 123003 (2015).
- [12] S. Camp, K.J. Schafer, and M.B. Gaarde, *Phys. Rev. A* **92**, 013404 (2015).
- [13] Y. Shao, M. Li, M.-M. Lin, X. Sun, X. Xie, P. Wang, Y. Deng, C. Wu, Q. Gong, and Y. Liu, *Phys. Rev. A* **92**, 013415 (2015).
- [14] L. Fechner, N. Camus, A. Krupp, J. Ullrich, T. Pfeifer, and R. Moshhammer, *Phys. Rev. A* **92**, 051403 (2015).
- [15] M. Li, P. Zhang, S. Luo, Y. Zhou, Q. Zhang, P. Lan, and P. Lu, *Phys. Rev. A* **92**, 063404 (2015).
- [16] T. Bredtmann, S. Chelkowski, A.D. Bandrauk, and M. Ivanov, *Phys. Rev. A* **93**, 021402 (2016).
- [17] M. Fushitani, C.N. Liu, A. Matsuda, T. Endo, Y. Toida, M. Nagasano, T. Togashi, M. Yabashi, T. Ishikawa, Y. Hikosaka, T. Morishita, and A. Hishikawa, *Nat. Photon.* **10**, 102 (2016).
- [18] H. Lv, W. Zuo, L. Zhao, H. Xu, M. Jin, D. Ding, S. Hu, and J. Chen, *Phys. Rev. A* **93**, 033415 (2016).
- [19] E.E. Serebryannikov and A.M. Zheltikov, *Phys. Rev. Lett.* **116**, 123901 (2016).
- [20] N.A. Hart, J. Strohhaber, A.A. Kolomenskii, G.G. Paulus, D. Bauer, and H.A. Schuessler, *Phys. Rev. A* **93**, 063426 (2016).
- [21] L.N. Li, J.P. Wang, and F. He, *J. Opt. Soc. Am. B* **33**, 1588 (2016).
- [22] W.-H. Xiong, X.-R. Xiao, L.Y. Peng, and Q. Gong, *Phys. Rev. A* **94**, 013417 (2016).
- [23] S. Beaulieu, S. Camp, D. Descamps, A. Comby, V. Wanie, S. Petit, F. Legare, K.J. Schafer, M.B. Gaarde, F. Catoire, and Y. Mairesse, *Phys. Rev. Lett.* **117**, 203001 (2016).
- [24] S. Larimian, S. Erattupuzha, C. Lemell, S. Yoshida, S. Nagele, R. Maurer, A. Baltuska, J. Burgdörfer, M. Kitzler, and X. Xie, *Phys. Rev. A* **94**, 033401 (2016).
- [25] H. Zimmermann, S. Patchkovskii, M. Ivanov, and U. Eichmann, *Phys. Rev. Lett.* **118**, 013003 (2017).
- [26] S. Bengtsson, E.W. Larsen, D. Kroon, S. Camp, M. Miranda, C.L. Arnold, A. L’Huillier, K.J. Schafer, M.B. Gaarde, L. Rippe, and J. Mauritsson, *Nat. Photon.* **11**, 252 (2017).
- [27] X. Gao, G. Patwardhan, S. Schrauth, D. Zhu, T. Popmintchev, H.C. Kapteyn, M.M. Murnane, D.A. Romanov, R.J. Levis, and A.L. Gaeta, *Phys. Rev. A* **95**, 013412 (2017).
- [28] I.A. Ivanov, C.H. Nam, and K.T. Kim, *Phys. Rev. A* **95**, 053401 (2017).
- [29] M. Ilchen, N. Douguet, T. Mazza, A.J. Rafipoor, C. Callegari, P. Finetti, O. Plekan, K.C. Prince, A. Demidovich, C. Grazioli, L. Avaldi, P. Bolognesi, M. Coreno, M. Di Fraia, M. Devetta, Y. Ovcharenko, S. Düsterer, K. Ueda, K. Bartschat, A.N. Grum-Grzhimailo, A.V. Bozhevolnov, A.K. Kazansky, N.M. Kabachnik, and M. Meyer, *Phys. Rev. Lett.* **118**, 013002 (2017).
- [30] C.A. Mancuso, K.M. Dorney, D.D. Hickstein, J.L. Chaloupka, X.-M. Tong, J.L. Ellis, H.C. Kapteyn, and M.M. Murnane, *Phys. Rev. A* **96**, 023402 (2017).
- [31] W.-H. Xiong, J.-Z. Jin, L.-Y. Peng, and Q. Gong, *Phys. Rev. A* **96**, 023418 (2017).
- [32] B. Piraux, F. Mota-Furtado, P.F. O’Mahony, A. Galstyan, and Yu. V. Popov, *Phys. Rev. A* **96**, 043402 (2017).
- [33] E.S. Toma, Ph. Antoine, A. de Bohan, and H.G. Müller, *J. Phys. B: At. Mol. Opt. Phys.* **32**, 5843 (1999).
- [34] X.-B. Bian and A.D. Bandrauk, *Phys. Rev. Lett.* **105**, 093903 (2010).
- [35] K. Krajewska, I.I. Fabrikant, and A.F. Starace, *Phys. Rev. A* **86**, 053410 (2012).
- [36] D.G. Arbo, K.I. Dimitriou, E. Persson, and J. Burgdörfer, *Phys. Rev. A* **78**, 013406 (2008).
- [37] S. Balay, S. Abhyankar, M.F. Adams, J. Brown, P. Brune, K. Buschelman, L. Dalcin, V. Eijkhout, W.D. Gropp, D. Kaushik, M.G. Knepley, L.C. McInnes, K. Rupp, B.F. Smith, S. Zampini, and H. Zhang, *PETSc Users Manual*, (ANL-95/11 - Revision 3.7), 2016.
- [38] S. Balay, W.D. Gropp, L.C. McInnes, and B.F. Smith, *Modern Software Tools in Scientific Computing*, edited by E. Arge, A.M. Bruaset, and H.P. Langtangen (Birkhäuser Press, 1997) p 163–202.
- [39] V. Hernandez, J.E. Roman, and V. Vidal, *ACM Trans. Math. Software*, **31**, 351–362, (2005).
- [40] J.E. Roman, C. Campos, E. Romero, and A. Tomas, *SLEPc Users Manual*, (DSIC-II/24/02 - Revision 3.7), 2016.
- [41] F. He, C. Ruiz, A. Becker, and U. Thumm, *J. Phys. B: At. Mol. Opt.* **44**, 211001 (2011).
- [42] X. Zhao, J. Chen, P. Fu, X. Liu, Z. Yan, B. Wang, *Phys. Rev. A* **87**, 043411 (2013).
- [43] X. Zhao, Y. YU-Jun, L. Xue-Shen, W. Bing-Bing, *Chin. Phys. Lett.* **31**, 043202 (2014).